ORIGINAL RESEARCH (AR) DOI: 10.4274/jems.2023.35761

Journal of ETA Maritime Science 2023;11(2):110-118

Advancing Computational Hydroacoustics for Marine Propellers: Investigating the Limits of Incompressible Solvers in Far-Field Noise Prediction

Ömer Kemal Kınacı[1], Cihad Delen[2]

[1]İstanbul Technical University, Department of Shipbuilding and Ocean Engineering, İstanbul, Türkiye
[2]İstanbul Technical University, Department of Naval Architecture and Marine Engineering, İstanbul, Türkiye

Abstract

As sound is a propagating pressure wave, it is important to obtain the hydrodynamic pressure oscillations in the fluid to calculate propeller noise. Numerical hydroacoustic simulations generally assume incompressible flow. Time delays in sound propagation are neglected due to the incompressibility assumption, leading to physically infeasible results in the far field. However, recent works have shown that incompressible solvers can comfortably be used in the near field. This work focused on the effect of distance on the accuracy of the incompressible solver and investigated the hydrodynamic and hydroacoustic properties of a model-scale Duisburg Test Case (DTC) propeller by the finite volume-based computational method. Open-water experiments on a 1/59.407 model-scale DTC propeller were carried out at the Ata Nutku Ship Model Testing Laboratory in Istanbul Technical University. Open-water numerical simulations were performed to determine the hydrodynamic and hydroacoustic properties of the propeller and validated with the hydrodynamic performance of the open-water propeller. Thrust and torque coefficients and open-water efficiency were compared with experiments. The Ffowcs-Williams and Hawkings equation was coupled with the incompressible solver using impermeable surfaces in hydroacoustic predictions of the hybrid solver. Pressure oscillations in the time domain at 21 receivers were used to calculate the sound pressure levels in the vicinity of the propeller. Results of incompressible and hybrid solvers were compared to determine the reach of incompressible solvers for hydroacoustic predictions. It was revealed that discrepancy starts after a 1.5-2D propeller.

Keywords: Ffowcs-Williams and Hawkings, Underwater acoustics, Propeller noise, Open-water propeller, Numerical hydroacoustics

1. Introduction

Noise emanating from ship propellers can be predicted by computational fluid dynamics approaches. Combined with robust turbulence modeling, finite volume-based methods have started dominating hydroacoustic predictions in the last two decades. A pioneering study in this field [1] implemented the boundary element method to solve for the flow around a marine propeller; however, recent works have used Reynolds-averaged Navier-Stokes equations (RANSEs). Resolving pressures in the flow field are mandatory to compute sound pressure levels; the RANSE is very effective in resolving the pressure field in the vicinity of propellers, but moving away from the cylinder loses its effectiveness. To solve this, the RANSE is combined with the Ffowcs-Williams and Hawkings (FWH) equation to calculate the pressure in the far field. Then, a substantial question can be raised: How far can we go from a noise source using incompressible solvers?

Sound travels through water due to the alternate compression and decompression of water molecules. Compressible flow can be solved by finite volume-based computational tools, which are very costly. When implementing incompressible solvers for noise calculation, time delays are ignored due to the travel of sound. The FWH equation emerges just at this point: it adds compressibility effects to incompressible solvers to account for time shifts. Incompressible solvers

Address for Correspondence: Ömer Kemal Kınacı, İstanbul Technical University, Department of Shipbuilding and Ocean Engineering, İstanbul, Türkiye
E-mail: kinacio@itu.edu.tr
ORCID ID: orcid.org/0000-0002-2956-9562

Received: 25.01.2023
Last Revision Received: 10.04.2023
Accepted: 19.04.2023

To cite this article: Ö.K. Kınacı, and C. Delen. "Advancing Computational Hydroacoustics for Marine Propellers: Investigating the Limits of Incompressible Solvers in Far-Field Noise Prediction." *Journal of ETA Maritime Science*, vol. 11(2), pp. 110-118, 2023.

are sufficient for near-field noise calculation, but for far-field noise calculation, they must be coupled with the FWH equation.

Transmission losses in underwater acoustic recordings are calculated for the correct noise estimation. Measurements and calculations are generally performed for receivers in the near field, and the general practice is to adopt the ITTC distance normalization equation [2] to exclude the effect of distance. This approach may provide a general idea about noise, however; it cannot be rated as entirely correct. The ITTC distance normalization equation is based on the inverse-square law method and is valid for point noise sources in stationary flow, while a ship propeller is a moving body consisting of many surfaces [3]. Thus, the sole implementation of incompressible solvers (with the inverse-square law method to carry results to the far field) will lead to crippled results after a certain distance.

In this work, the range of applicabilities of incompressible solvers for hydroacoustic predictions of marine propellers were studied. Comparison of computational results with the hybrid solver was made, in which the FWH-RANSE equation includes the time delay effect. The hull greatly contributes to the hydrodynamic performances of propellers [4], but hydroacoustic properties are not [5]. The scattering effect due to the hull is negligible in propeller near-field sound properties [6]; hence, only open-water propellers were involved. Numerical results were first validated by the hydrodynamic performance of the propeller in open water using experiments from two different laboratories. Cavitation was not included. The advance coefficient of the propeller in numerical simulations is rather high $J = 0.8$, at which higher noise levels are expected at the propeller disk [7].

2. Open-Water Experiments on the Propeller

Open-water experiments were performed for a 1/59.407 model-scale DTC propeller with fixed-pitch five blade, a geometry very close to the Wageningen Propeller B-Series, a propeller geometry very similar to that of the KCS propeller [8]. The propeller has open-water test results at this model scale, as shown in previous work [9]. Comparisons have also been done with the KCS propeller [10]. Table 1 lists the geometric properties of the propeller.

The propeller was manufactured with a high-precision three-dimensional printer that could use PLA, ABS, and TPU filaments and has a printing volume of 200 mm × 200 mm × 200 mm. To obtain high surface sensitivity, a thin layer of paste and sanding were applied first on the propeller surface followed by painting (Figure 1) before readying for the experiments.

Table 1. *Geometric properties of the DTC propeller*

Type	Fixed-pitch
No. of blades	5
P/D $(0.7R)$	0.959
A_E/A_0	0.8
Direction of rotation	Right-handed
Hub ratio	0.176
Diameter	0.15 m

Figure 1. *DTC propeller geometry*

DTC: Duisburg Test Case

The experiments were conducted at the Ata Nutku Ship Model Testing Laboratory in İstanbul Technical University. Recommendations and procedures of the ITTC [11] on conducting open-water experiments were followed during the tests. A ship model was used to determine the open-water performance of the model propeller. The electric motor, dynamometer, shaft, and propeller, which are the experimental setup, were placed in the model. The model propeller was extended with the help of a shaft to a distance that will not be affected by the hull. The propeller was placed in front of the model so that the model velocity is equal to the flow velocity on the propeller. In this way, the inflow to the propeller is uniform and homogeneous. The propeller center was submerged to at least $1.5D$ under the free surface that it is not affected by the free water surface. The propeller's flow rate, propeller revolution rate (n), thrust (T), and torque (Q) were simultaneously stored. Open-water experiments were performed in a wide J range corresponding to constant velocity and variable revolution rate. The experiments were then repeated for the same case without the propeller, and necessary corrections were made on the raw results. The propeller was connected to

an electric motor via a shaft and submerged to at least $1.5D$ under the water. The experiments were then repeated for the same case without the propeller, and necessary corrections were made on the raw results.

The force and moment generated by the propeller were measured using a multicomponent sensor. Thrust T and torque Q read from the sensor were nondimensionalized by the following equations:

$$K_T = \frac{T}{\rho n^2 D^4} \quad (1)$$

$$K_Q = \frac{Q}{\rho n^2 D^5} \quad (2)$$

where n, ρ, and D refer to the propeller rotation rate, fluid density, and propeller diameter to obtain the thrust and torque coefficients denoted by K_T and K_Q, respectively. The open-water propeller efficiency was calculated using

$$\eta_0 = \frac{J}{2\pi}\frac{K_T}{K_Q} \quad (3)$$

3. Details of the Numerical Simulations

Numerical simulations of the open-water propeller were conducted using a fluid domain consisting of two interbedded cylinders. The outer cylinder covers the whole fluid domain, and the inner cylinder covers the rotating domain. The whole fluid domain has a diameter of $10D/3$ and a length of $100D/3$. The propeller is surrounded by the inner cylinder that has a diameter of $4D/3$ and a length of $10D/3$. This rotating domain is given a rotation rate to represent the propeller rotation. Hydroacoustic analysis is more dependent on grid resolution than hydrodynamic analysis [12]; therefore, more elements than conventional open-water performance tests were used. There are 3.82M elements in the whole domain, including the 2.4M in the rotating domain. The boundary layer close to the propeller was discretized by 6 prism layers to introduce viscous effects. Grid refinements were applied to the hydrophone locations to obtain a better pressure field using the incompressible solver. A plane section of the grid structure at $y = 0$ is given in Figure 2. Locations of the 21 hydrophones in the domain are shown by red dots in this figure above the propeller.

Numerical hydroacoustic simulations are conducted for the $1/59.407$ model-scale propeller in open water. This model scale corresponds to a propeller diameter of $D = 15$ cm. The surfaces of the inner circle surrounding the propeller are defined as the interface between the dynamic (rotating) and static (no rotation) domains. The outer cylindrical domain has two different boundary conditions. The inlet and the side wall are defined as "velocity inlet," while the outlet is defined as "pressure outlet." The fluid is flowing in the $-x$ direction. The rotation rate applied on the inner circle (rotating domain) and the velocity defined for the velocity inlet boundary condition are given in Table 2.

The turbulent flow around the propeller is simulated using the $k-\varepsilon$ turbulence model [13]. The simulation is set to be transient to obtain the fluctuations in hydrodynamic

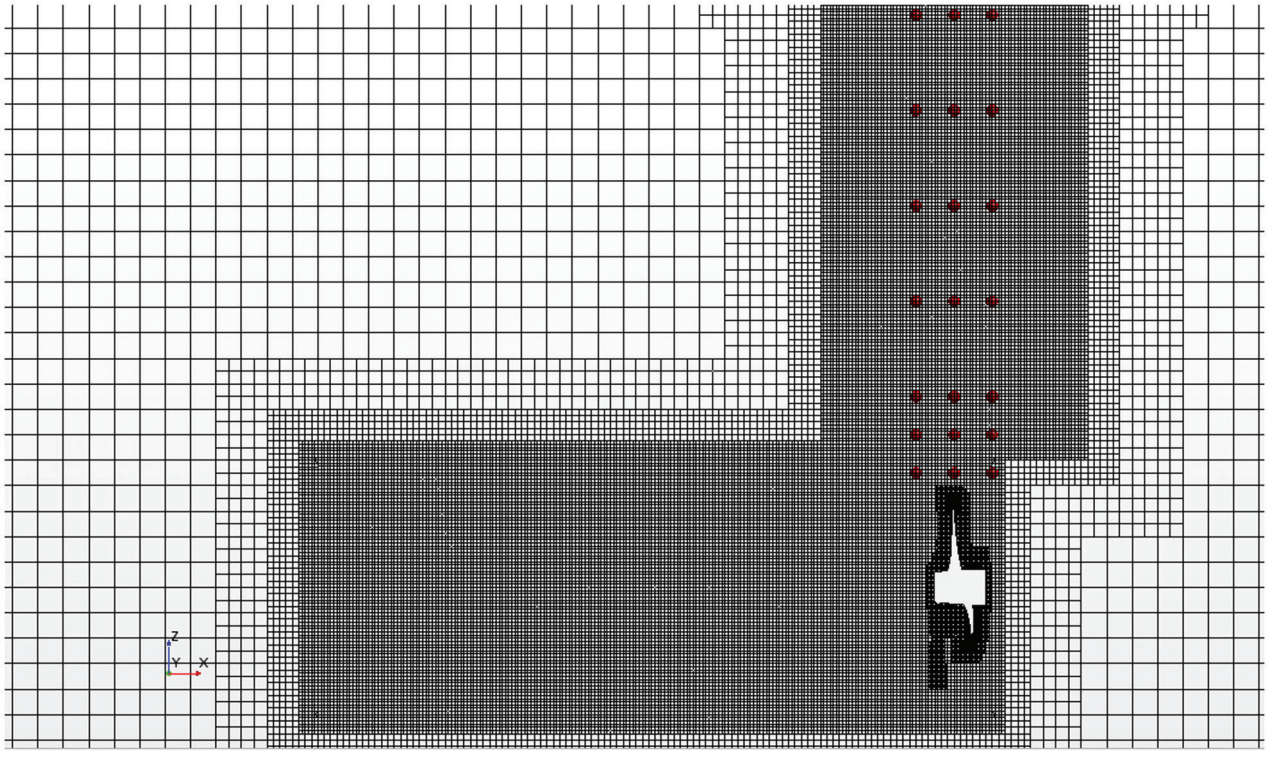

Figure 2. *View of the part of the grid structure implemented in the fluid domain. The grid was refined in hydrophone positions (red dots) to obtain sensitive pressure results with the incompressible solver*

Table 2. *Simulation parameters for the open-water propeller test*

Propeller diameter, D (m)	Propeller rotation rate, n (rps)	Flow velocity, V (m/s)	Propeller advance ratio, J (-)
0.15	13.9	1.668	0.8

pressure in the time domain. The time step size is selected using the formulation given elsewhere [3]:

$$\Delta t \leq_{k \cdot BPF} \frac{1}{} \quad (4)$$

The blade passage frequency of the simulation in this study is $BPF = n \cdot Z = 13.9 \cdot 5 = 69.5Hz$. The constant in the time step size formulation is taken as $k = 9$ in the reference study. In this case, the time step size should be $\Delta t \leq 0.0016s$. To obtain smooth pressure curves, the time step size was selected to be $\Delta t = 7.5 \cdot 10^{-4} s$.

In the simulations, the flow is assumed to be incompressible. Throughout the paper, "FWH" means that the FWH equation is coupled with the incompressible solver. This hybrid method uses the inner surface surrounding the propeller as an "impermeable" surface and solves the equation:

$$\bar{\mathbb{D}}^2 p' = \frac{\partial}{\partial t}[\rho_0 \vec{v}\, \delta(f)\, \Delta f] - \nabla \cdot [P\, \delta(f)\, \Delta f] + \nabla \cdot \nabla \cdot [T\, H(f)] \quad (5)$$

This equation was first put forward by previous work [14] and later solved by another study [15] without considering the quadrupole terms. Mathematically, the monopole and dipole sources are defined using the Green function:

$$4\pi p'_T(x,t) = \int_{f=0} \left[\frac{\rho_0\, v_n}{r(1-M_r)^2} + \frac{\rho_0\, v_n \dot{r_i} \dot{M_i}}{r(1-M_r)^3}\right]_{ret} dS + \int_{f=0} \left[\frac{\rho_0 c\, v_n (M_r - M^2)}{r^2(1-M_r)^3}\right]_{ret} dS \quad (6)$$

$$4\pi p'_L(x,t) = \int_{f=0} \left[\frac{\dot{P}\cos\theta}{cr(1-M_r)^2} + \frac{\dot{r_i} M_i P \cos\theta}{cr(1-M_r)^3}\right]_{ret} dS + \int_{f=0} \left[\frac{P(\cos\theta - M_i n_i)}{r^2(1-M_r)^2} + \frac{(M_r - M^2) P \cos\theta}{r^2(1-M_r)^3}\right]_{ret} dS \quad (7)$$

For the definition of the relevant parameters in these two equations and their derivations, readers are referred to the reference report [15]. Locations of the hydrophones are generally selected on (or close to) the propeller disk for hydroacoustic calculations. This is due to the incapability of RANSE in resolving the chaotic flow in the wake of the propeller [16]. The flow was sent to the propeller rotating at a constant rate in the $-x$ direction, and pressure fluctuations were calculated at 21 points in the vicinity of the propeller disk. Figure 3 shows the locations of the hydrophones (the figure is rotated to save space).

4. Results

Numerical simulation results validated with open-water propeller experiments conducted in two different laboratories are presented followed by, after observing a good match, predictions of propeller noise at different locations in the flow.

4.1. Hydrodynamic Validation with Experiments

Despite recent efforts to improve the hydroacoustic testing capabilities of towing tanks [17], it is still not convenient to measure noise in long but narrow tanks due to possible reverberation effects from side walls [15]. Thus, in this work, the numerical approach was only validated with the hydrodynamic aspects of flow, which only considers the thrust and torque generated by the propeller. The open-water propeller tests in previous work [9] were conducted at the Ata Nutku Ship Model Testing Laboratory in İstanbul Technical University. Figure 4 illustrates the results.

This is an indirect way of validating computational hydroacoustic results, but it is indeed one of the best methods for the assessment of numerical simulations. Finite volume-based methods use the Navier-Stokes equations to solve for the pressure applied on the body to calculate the forces and moments acting on it. If the pressure on the body is accurate, then inherently forces and moments acting on the body will also be accurate. Considering that sound is a form of pressure wave and that the implemented finite volume-based method is good enough to solve for the pressure in the fluid domain, we can make an assessment that once the hydrodynamic aspects of a propeller are solved correctly, then hydroacoustic predictions are also valid. All results are in accordance with each other in Figure 4, and therefore, it is considered that the numerical simulation at $J = 0.8$ has enough accuracy to predict the noise levels of the propeller.

4.2. Hydroacoustic Predictions

Investigation of the pressure oscillations in the time domain for 21 hydrophones will reveal the effects of the incompressibility assumption in the flow, the effect of the axial distance to the noise source, and the effect of the radial distance to the noise source.

To understand the effect of the axial distance, hydrodynamic pressures in the time domain for the closest hydrophones were investigated. Figure 5 gives the pressure oscillations in the time domain and sound pressure levels in the frequency domain for HP1, HP2, and HP3.

As noted in previous sections, numerical simulations were conducted at $n = 13.9$ rps. Considering the five blades $Z = 5$ of the DTC propeller used here, the blade passage frequency becomes $BPF = n \cdot Z = 69.5$ Hz. Thus, we expect the subharmonic to be at the propeller rotation rate n, which is 13 Hz, the first harmonic to be at BPF, which is 69.5 Hz, and the second harmonic to be double the BPF, which makes 139 Hz.

The subharmonic, the first harmonic, and the second harmonic are all visible for all the hydrophones given in Figure 5. Due to being located at the propeller disk, HP2 has

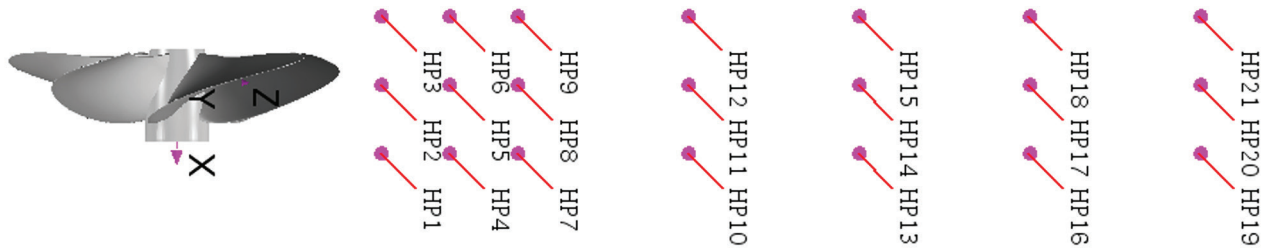

Figure 3. *Locations of the hydrophones in the fluid domain*

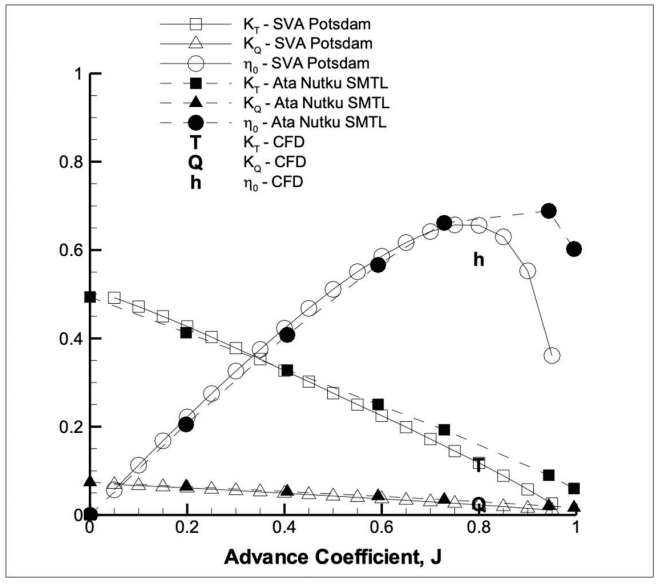

Figure 4. *Open-water experiments at two different towing tanks in comparison with the numerical simulation at J = 0.8*

the largest oscillations in pressure, leading, as a return, to higher sound pressure levels. HP1 and HP3 are equidistant to the propeller disk. As observed from the graphs, pressure oscillations (and inherently sound pressure levels) are similar for these two hydrophones. Thus, if the axial distances are similar, sound pressure levels are also similar regardless of the receiver being located upstream or downstream. These three hydrophones are located closest to the propeller, considered to be in the near field. Results obtained by the hybrid solver (FWH) are in line with the results of the incompressible solver (RANSE), which is expected. The first harmonic is dominant in the sound pressure levels, which corresponds to the blade passage frequency of the propeller. The effect of radial distance from the noise source is investigated in Figure 6 using the pressure oscillations obtained from HP5, HP11, and HP20.

All hydrophones given in Figure 6 lie on the propeller disk. We start to see deviations between the incompressible solver (RANSE) and the hybrid solver (FWH) as we move away from the propeller tip. Results are compatible in HP5 but quite different in HP2, which leads us to the conclusion that time shifts start playing a significant role in sound transmission. Pressure oscillations tend to get smaller as the distance increased from the propeller. This is also observable from the sound pressure levels in the frequency domain: noise levels are distinguishably lower. Another thing to note from this figure is that the first harmonic is dominant in the near-field, while it is subharmonic in the far-field. The effects of the first and the second harmonics nearly vanish in HP20 in FWH-based results. On the contrary, the incompressible solver (RANSE) still shows a significant level of the first harmonic in the frequency domain, but this is considered to be due to turbulence dissipation [18]. Table 3 lists the dominant frequencies and sound pressure levels obtained using FWH.

To make a better assessment of the differences in the incompressible solver (RANSE) with the hybrid solver (FWH), sound pressure levels at the subharmonic, the first harmonic, and the second harmonic are extracted from the frequency domain and graphed with respect to the distance from the propeller, as shown in Figure 7. Although the subharmonic results are in good accordance regardless of the distance to the propeller (covered in this study), incompressible solver (RANSE) results are draw apart from the hybrid solver (FWH) for the first and second harmonics after $1.5–2D$ from the propeller. It should be kept in mind that cavitation does not exist in our case. In the presence of serious cavitation, the deviation could even start from the very near field [3].

The findings in this work indicate the necessity of adding compressibility effects in the far field. FWH is a supporting equation to add this particular effect on the incompressible solver. The incompressible solver is capable of generating accurate results in the immediate vicinity but becomes inadequate as the distance over which sound travels increases. RANSE, by itself, cannot handle the first and second harmonics of the sound pressure as the results start deviating after a certain distance. The accordance of subharmonic results is considered to be within an acceptable range, but the differences in the other harmonics lead to erroneous calculations of the overall sound pressure levels generated within the fluid.

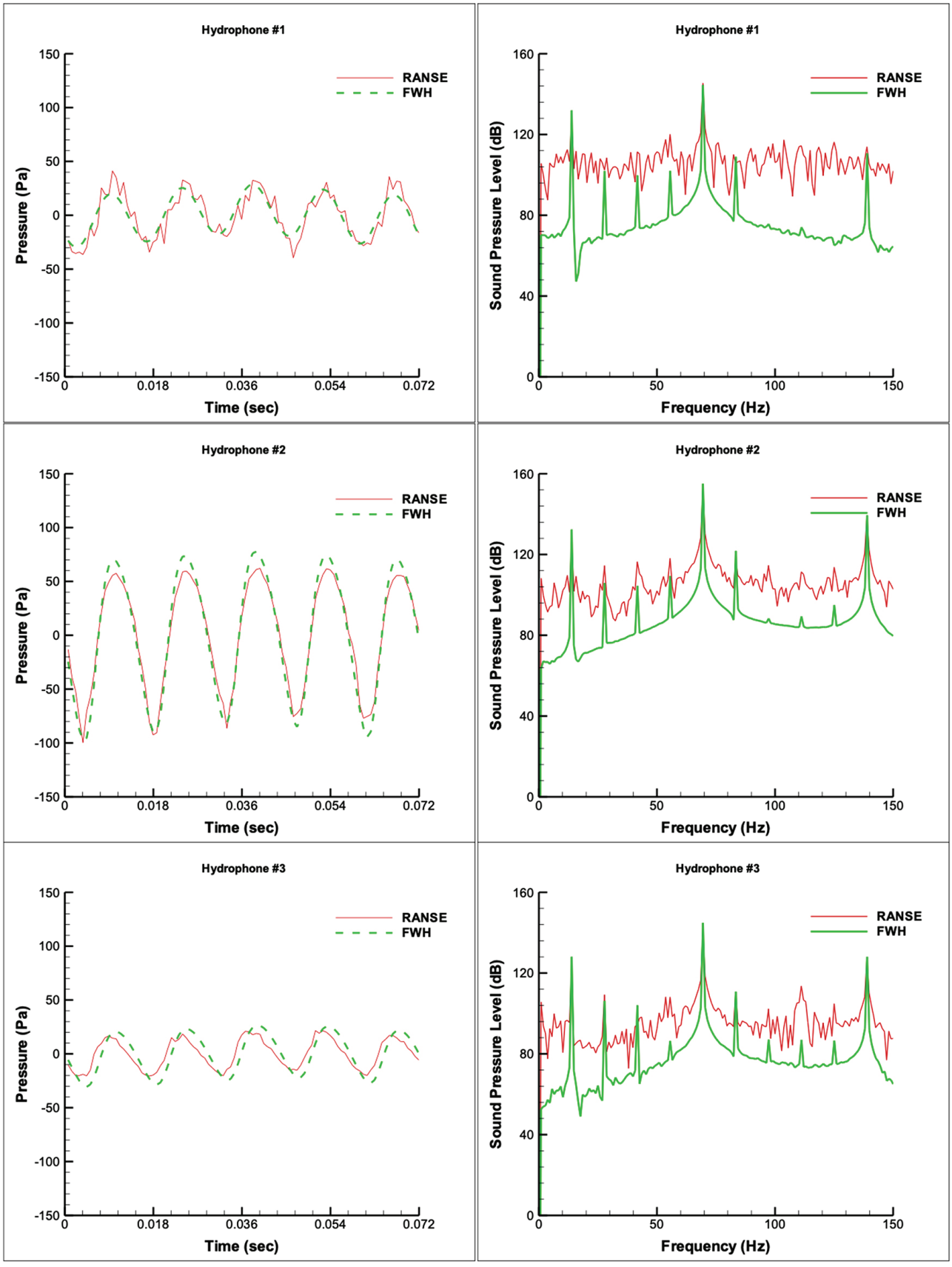

Figure 5. *Pressure oscillations in time domain for HP1, HP2 and HP3 (left). Sound pressure levels in frequency domain for the same hydrophones (right)*

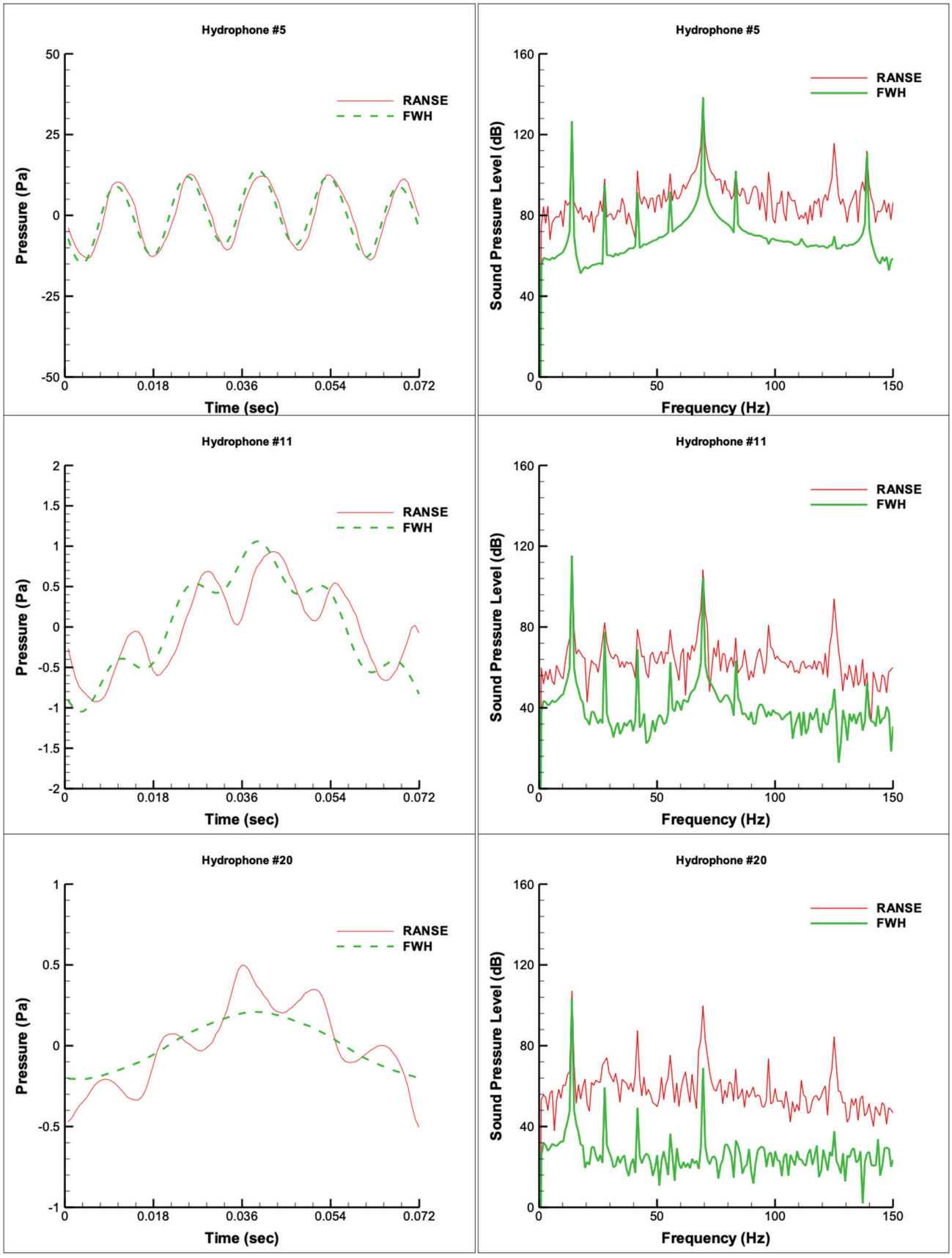

Figure 6. *Pressure oscillations in time domain for HP5, HP11 and HP20 (left). Sound pressure levels in frequency domain for the same hydrophones (right)*

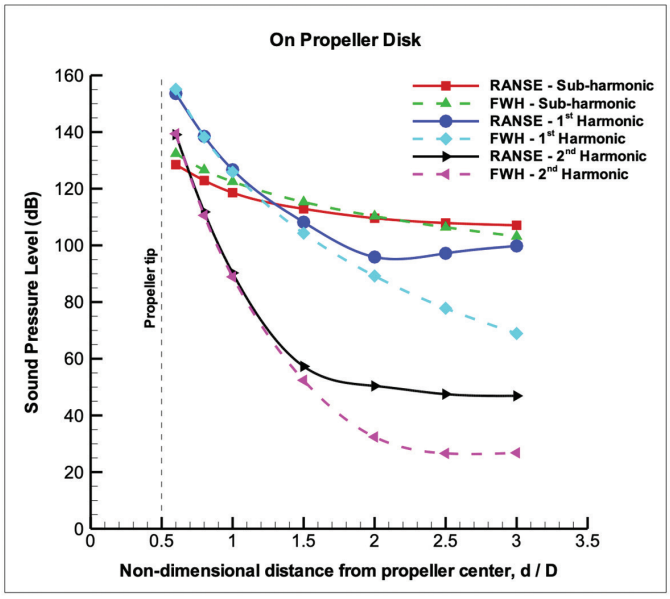

Figure 7. *Subharmonic, first harmonic, and second harmonic results obtained by RANSE and FWH with respect to the distance from the noise*

RANSE: Reynolds-averaged Navier-Stokes equations, FWH: Ffowcs-Williams and Hawkings

Table 3. *Dominant frequencies and sound pressure levels at the receivers*

Hydrophones	Dominant frequency	SPL (approximately)
HP1-HP9	First harmonic	135-150dB
HP10-HP21	Subharmonic	105-115dB

5. Conclusion

In this work, two different hydroacoustic models were tested on a model-scale DTC propeller with a finite volume-based computational method. The numerical approach was first validated by open-water experiments conducted at the Ata Nutku Ship Model Testing Laboratory and compared with the literature results. The hydrodynamic results of the open-water propeller were found to be compatible. After method validation, hydroacoustic results from the incompressible solver (RANSE) were compared with the hybrid solver (FWH). Assessments were made using pressure data from 21 hydrophones in the fluid domain.

The differences in results from the incompressible and hybrid solvers were investigated in the axial and radial directions. Both solvers generated similar results for receivers having equal axial distance to the noise source, regardless its location upstream or downstream. For hydrophones located in the propeller near-field, the incompressible and hybrid solvers are in good accordance. Numerical hydroacoustic simulations revealed that the first harmonic is dominant in sound pressure levels corresponding to the propeller's blade passage frequency but increasing radial distance from the source starts to show discrepancies.

Time delays due to compressibility start becoming a decisive factor in the results for the far field. While the incompressible and hybrid solvers generate similar results in the near field, deviations arise in the far field. Although the decrease in noise levels with increasing velocity is observable from both solvers, the incompressible solver starts generating unconceivable results in the far field. The first harmonic is dominant in the near field, which is clear in both solvers; however, the incompressible solver fails to capture the amplitudes of subharmonic frequencies after 1.5-2D from the propeller.

Future work is being done for conducting research on sound directivity (which is partially covered in this study). Moreover, sound pressure levels in the wake region of the propeller remain a concern using both solvers: more hydroacoustic simulations using advanced turbulence models such as LES, DES, or SAS are required to resolve the noise characteristics in this chaotic flow regime.

Acknowledgments

This work was supported by the Scientific and Technological Research Council of Türkiye (TÜBİTAK). Project ID: 218 M372.

Peer-review: Externally peer-reviewed.

Authorship Contributions

Concept design: Ö.K.K., C.D., Data Collection or Processing: Ö.K.K., Analysis or Interpretation: Ö.K.K., Literature Review: Ö.K.K., C.D., Writing, Reviewing and Editing: Ö.K.K., C.D.

Funding: The author(s) received no financial support for the research, authorship, and/or publication of this article

References

[1] H. Seol, B. Jung, J. C. Suh, and S. Lee, "Prediction of non-cavitating underwater propeller noise," *Journal of Sound and Vibration,* vol. 257, pp. 131-156, Oct 2002.

[2] ITTC, 2014. "Model scale noise measurements - 7.5-02-01-05". *ITTC - Recommended Procedures and Guidelines.*

[3] S. Sezen, and O. K. Kinaci, "Incompressible flow assumption in hydroacoustic predictions of marine propellers," *Ocean Engineering,* vol. 186, 106138, Aug 2019.

[4] S. E. Belhenniche, O. Imine, and O. K. Kinaci, "Hydrodynamic and hydroacoustic computational prediction of conventional and highly skewed marine propellers operating in non-uniform ship wake," *Journal of Marine Science and Application,* vol. 19, pp. 28-40, July 2020.

[5] Z. Q. Rao, and C. J. Yang, "Numerical prediction of tonal noise for non-cavitating propellers in effective wake," *Ships and Offshore Structures,* vol. 13, pp. 551-560, 2018.

[6] Y. Wei, et al. "Scattering effect of submarine hull on propeller non-cavitation noise," *Journal of Sound and Vibration,* vol. 370, pp. 319-335, May 2016.

[7] B. Mousavi, A. A. Rahrovi, and S. Kheradmand, "Numerical simulation of tonal and broadband hydrodynamic noises of non-cavitating underwater propeller," *Polish Maritime Research,* vol. 21, pp. 46-53, Oct 2014.

[8] D. Ozturk, C. Delen, S. E. Belhenniche, and O. K. Kinaci, "The effect of propeller pitch on ship propulsion," *Transactions on Maritime Science,* vol. 11, pp. 133-155, 2022.

[9] O. el Moctar, V. Shigunov, and T. Zorn, "Duisburg test case: post-panamax container ship for benchmarking," *Ship Technology Research,* vol. 59, pp. 50-64, 2012.

[10] SIMMAN2020 Conference Website. KCS Ship Data. [Online]. https://www.simman2020.kr/contents/KCS.php. [Accessed: Apr. 4, 2023].

[11] ITTC, 2017. "Open Water Test - 7.5-02-03-02.1". *ITTC - Recommended Procedures and Guidelines*.

[12] S. Sezen, T. Cosgun, A. Yurtseven, and M. Atlar, "Numerical investigation of marine propeller underwater radiated noise using acoustic analogy Part 1: The influence of grid resolution," *Ocean Engineering,* vol. 220, 108448, Jan 2021.

[13] S. Sezen, T. Cosgun, A. Yurtseven, and M. Atlar, "Numerical investigation of marine propeller underwater radiated noise using acoustic analogy Part 2: The influence of eddy viscosity turbulence models," *Ocean Engineering,* vol. 220, 108353, Jan 2021.

[14] J. E. Ffowcs Williams, and D. L. Hawkings. "Sound generation by turbulence and surfaces in arbitrary motion." Philosophical Transactions of the Royal Society of London. *Series A, Mathematical and Physical Sciences,* vol. 264, pp. 321-342, May 1969.

[15] F. Farassat, "Derivation of Formulations 1 and 1A of Farassat," NASA/TM-2007-214853. Langley Research Center, Hampton, Virginia, March 2007.

[16] S. Ianniello, R. Muscari, and A. Di Mascio, "Ship underwater noise assessment by the acoustic analogy. Part I: nonlinear analysis of a marine propeller in a uniform flow," *Journal of Marine Science and Technology,* vol. 18, pp. 547-570, July 2013.

[17] H. Way, P. Joseph, S. Turnock, R. Leung, and V. Humphrey, "Acoustic characterisation of towing tanks," *Ocean Engineering,* vol. 22, 108338, Jan 2021.

[18] T. Lloyd, D. Rijpkema, and E. van Wijngaarden, "Marine propeller acoustic modelling: comparing CFD results with an acoustic analogy method," *In Fourth International Symposium on Marine Propulsors,* Austin, Texas, May-June 2015.